Supplementary information for the manuscript

Out-of-Africa migration and Neolithic co-expansion of *Mycobacterium tuberculosis* with modern humans

Iñaki Comas[1,2@], Mireia Coscolla[3,4]*, Tao Luo[5]*, Sonia Borrell[3,4], Kathryn E. Holt[6], Midori Kato-Maeda[7], Julian Parkhill[8], Bijaya Malla[3,4], Stefan Berg[9], Guy Thwaites[10], Dorothy Yeboah-Manu[11], Graham Bothamley[12], Jian Mei[13], Lanhai Wei[14], Stephen Bentley[8], Simon R. Harris[8], Stefan Niemann[15], Roland Diel[16], Abraham Aseffa[17], Qian Gao[5@], Douglas Young[18,19#], Sebastien Gagneux[3,4#@]

This supplementary PDF file includes the following information:

Supplementary Figures 1-10

Supplementary Table 7

Supplementary Note

Note: Supplementary Tables 1,2,3,4,5,6 are provided as individual excel files

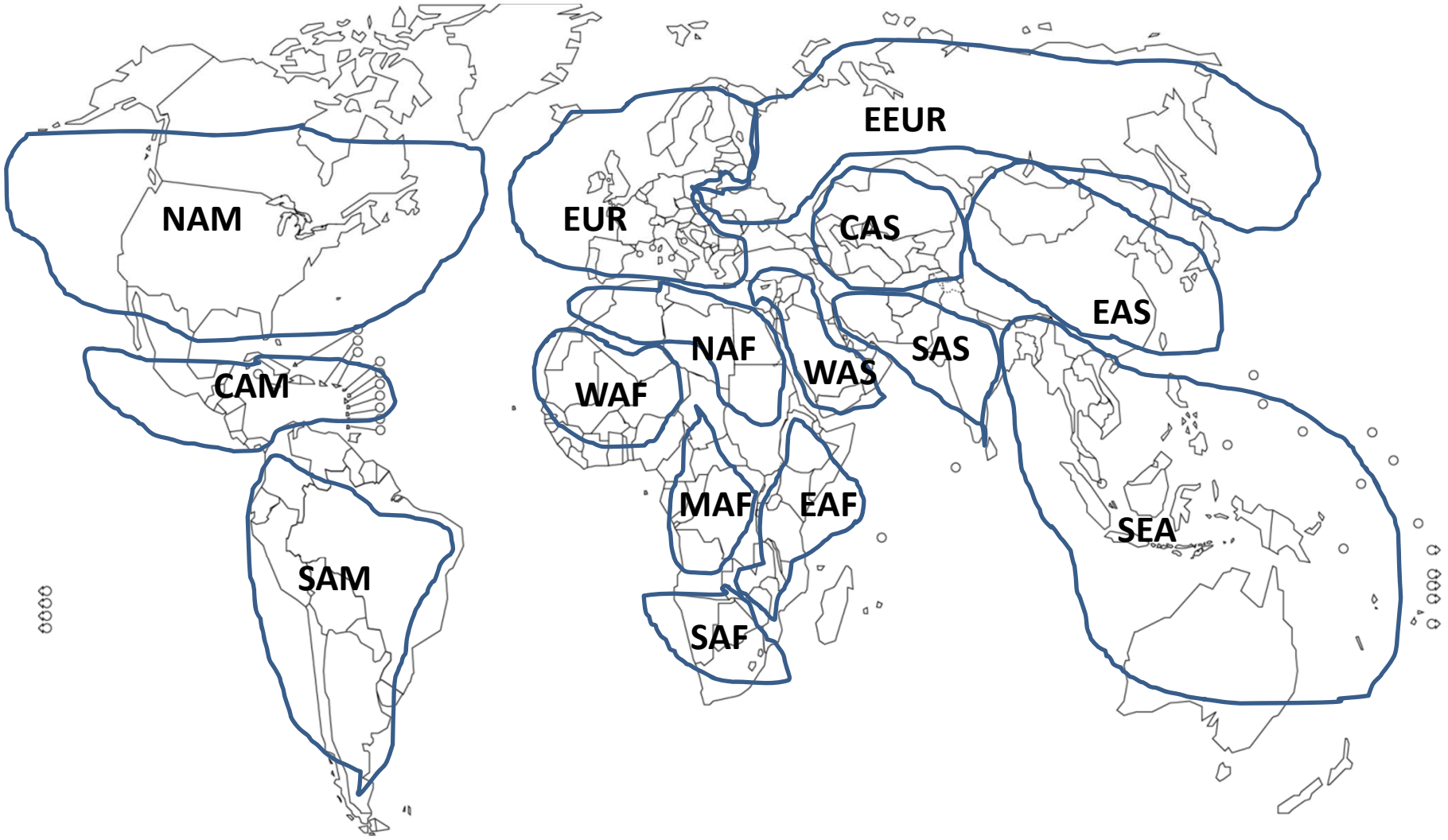

Supplementary Figure 1. Global geographic areas used for the phylogeographic analysis. These areas are based on the United Nation geographical sub-regions (note: some of these regions were not represented in the MTBC strain collection analyzed here). The regional code for the different areas reads as follows: CAM - Central America; CAS - Central Asia; EAF - East Africa; EAS - East Asia; EUR - Europe; EEUR – East Europe; MAF – Middle Africa; NAF – North Africa; NAM - North America; SAF - South Africa; SAM - South America; SAS - South Asia; SEA - South East Asia; WAF - West Africa; WAS - West Asia.

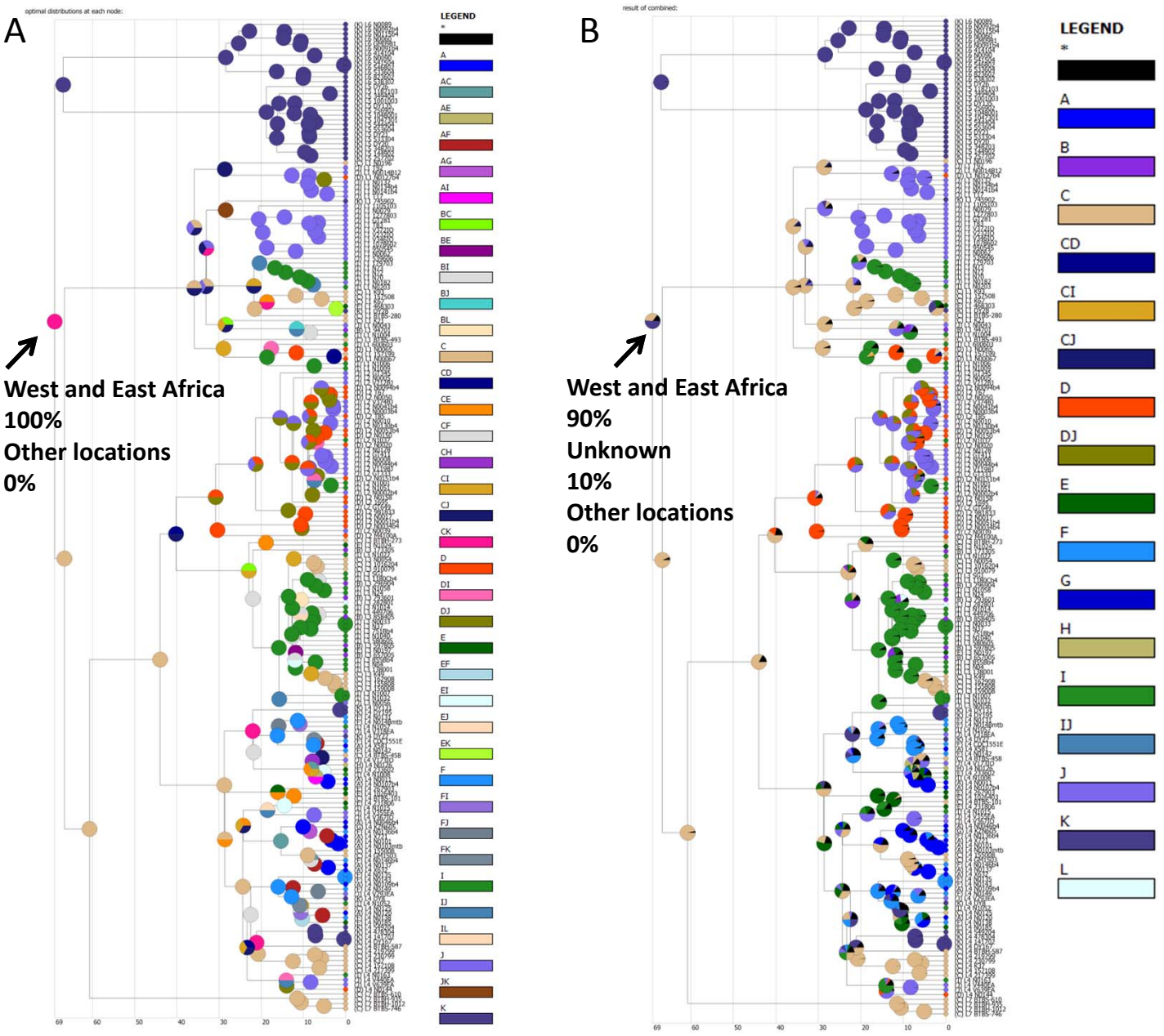

Area	Region code	Region name
A	CAM	Central America
B	CAS	Central Asia
C	EAF	East Africa
D	EAS	East Asia
E	EUR	Europe
F	NAM	North America
G	SAF	South Africa
H	SAM	South America
I	SAS	South Asia
J	SEA	Sout East Asia
K	WAF	West Africa
L	WAS	West Asia

Supplementary Figure 2. Results of the phylogeographic analysis using RASP. We used **(A)** a parsimony-based method called S-DIVA traditionally applied to species biogeography in the context of variance events and a Bayesian-based method **(B)**. Pie-charts reflect probability of the respective area. Areas are colour-coded as in the legends allowing for single or combined distributions. The probabilities for the root of the tree (the MRCA of the MTBC) are indicated in the corresponding node.

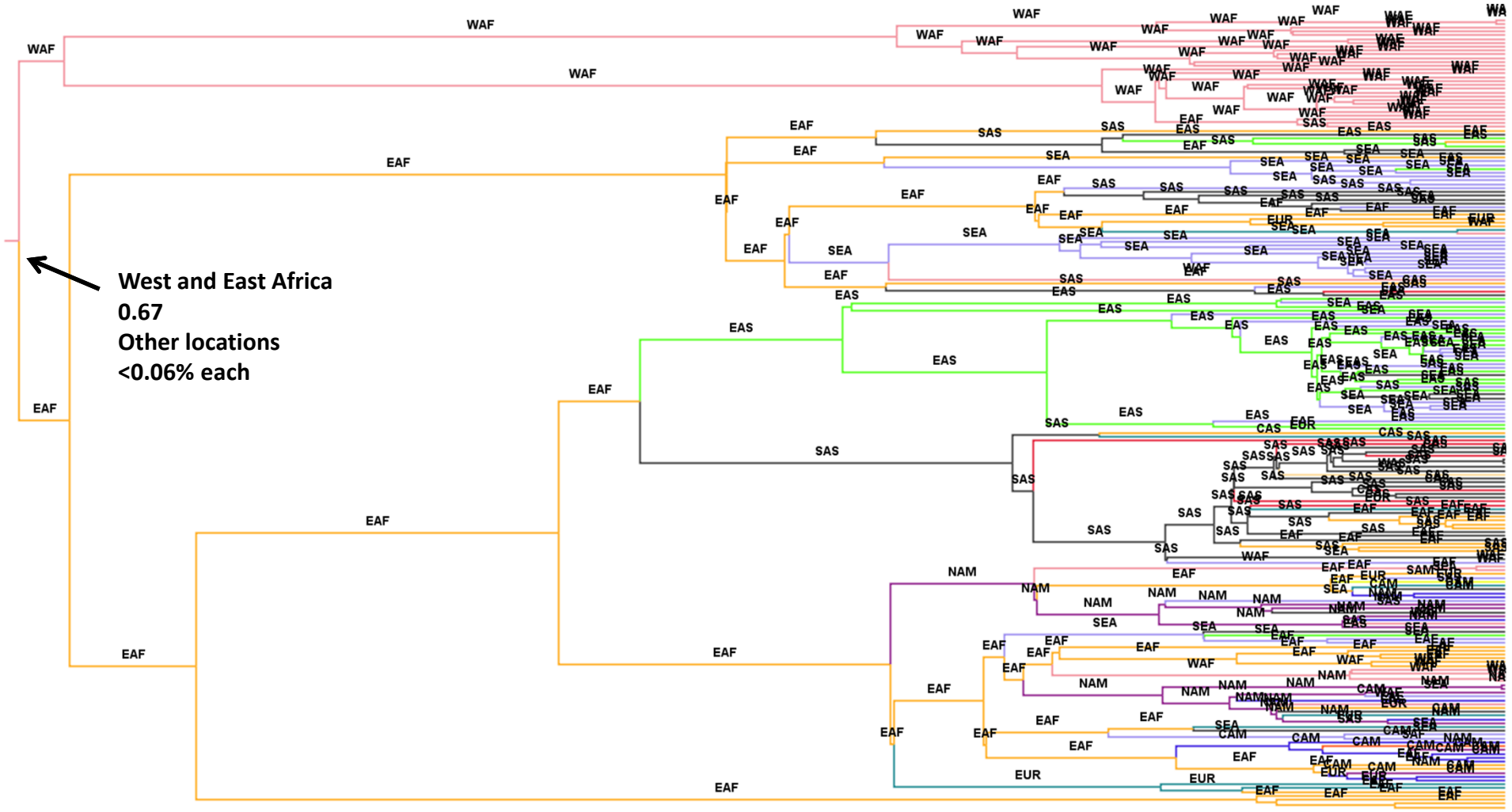

Supplementary Figure 3. Results of the phylogeographical analysis using the BSSVS procedure implemented in BEAST. Branches are colour-coded by the most likely geographic location of the internal nodes. The same information is given using the regional codes from Supplementary Fig. 2. The Bayesian posterior probability of the root (MRCA of the MTBC) is indicated.

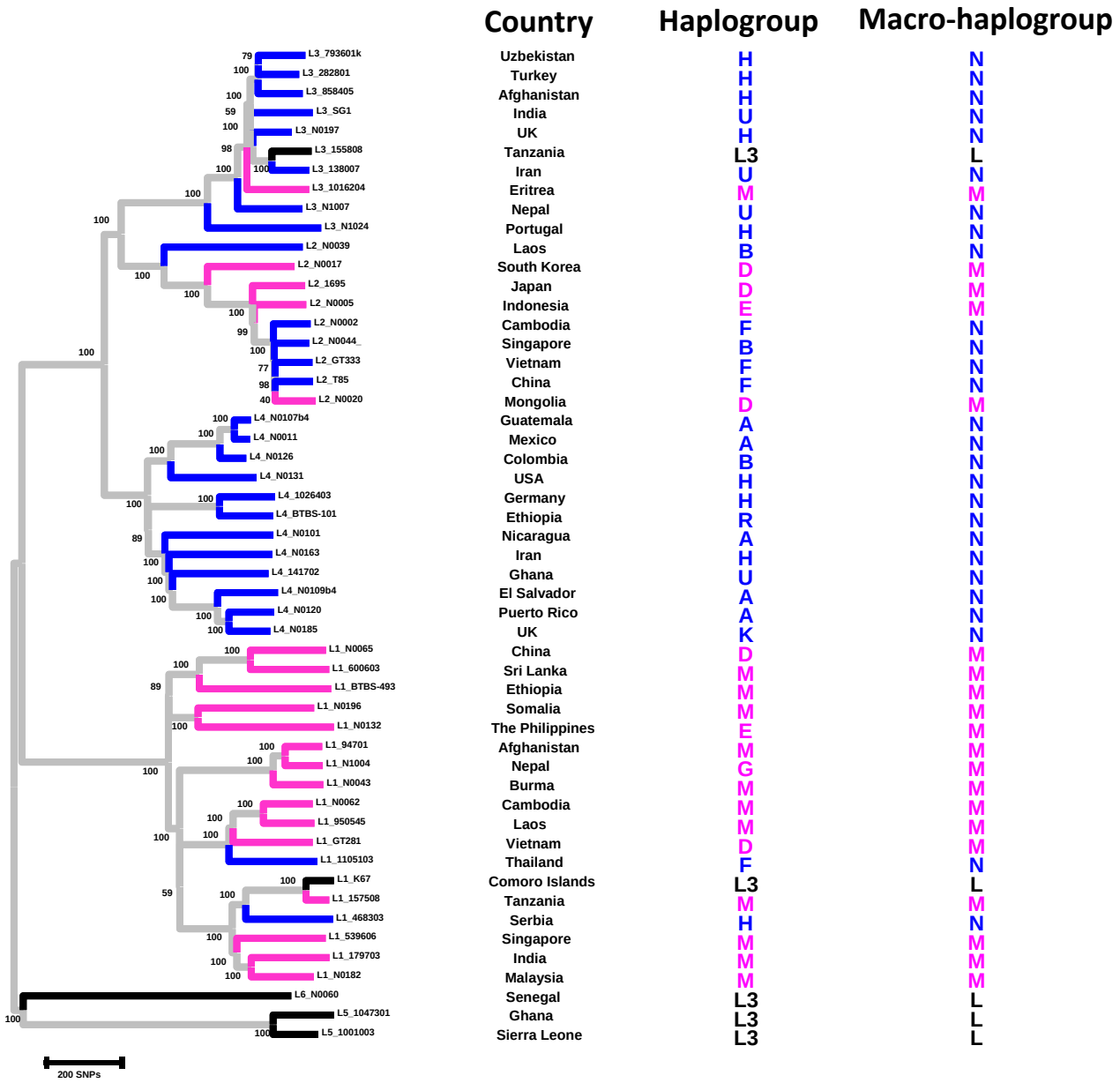

Supplementary Figure 4. MTBC phylogeny (Neighbour-joining, 1000 bootstraps, number of differences) used to test the phylogenetic association between MTBC and human mitochondrial groups. The country of origin of the patient is shown which was used to look for the most common mtDNA haplogroups (see Online methods for an explanation of the association tests used and references from 28-56 in the Supplementary Note for a list of references used). The branches in the tree are colour coded according to the matched macro-haplogroup (L, M, and N) of the corresponding MTBC strains.

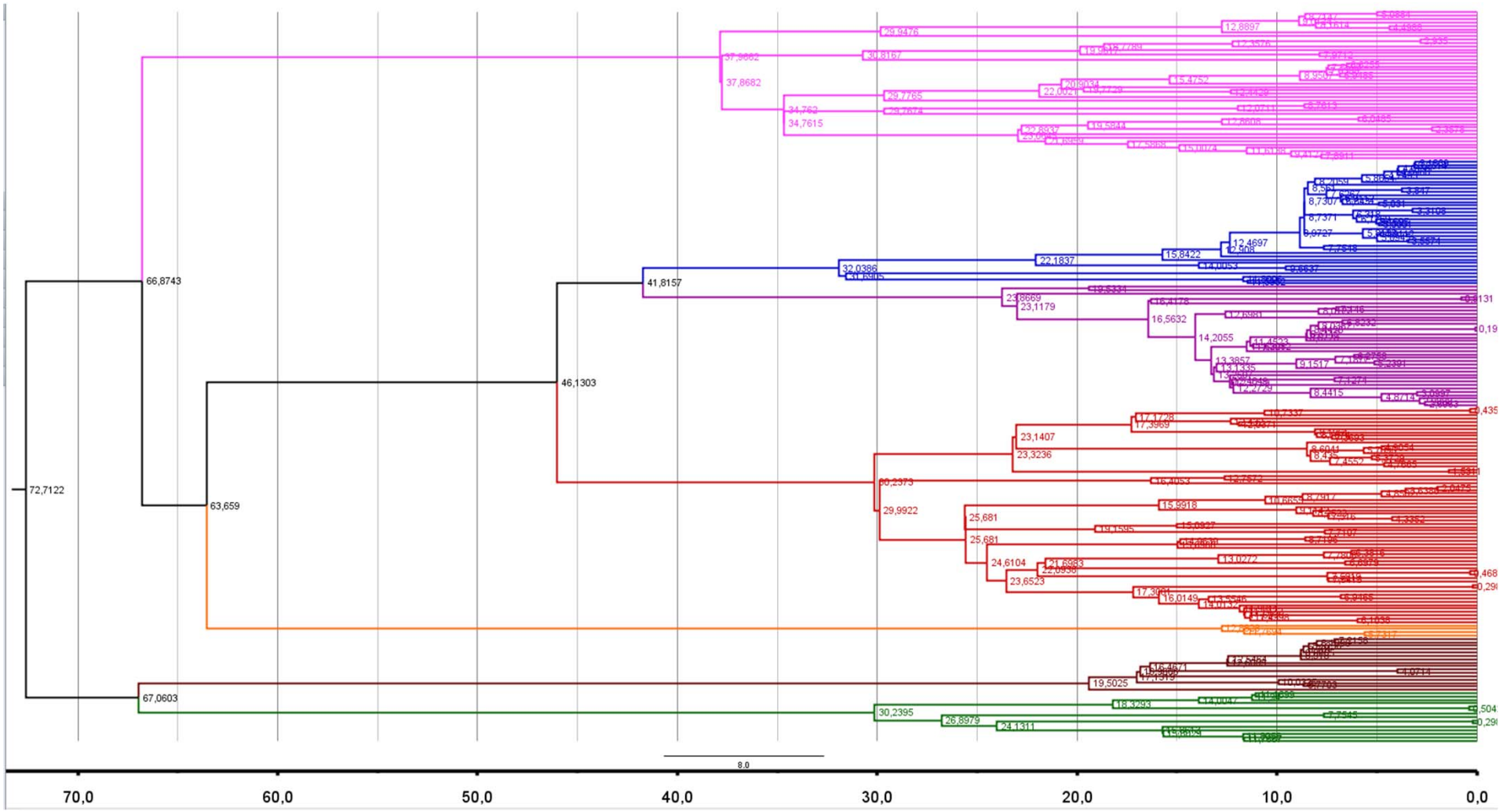

Supplementary Figure 5. BEAST result of the MTBC-70 model in which we assume a priori that the ancestor of MTBC existed sometime 70 kya. The numbers on the axis indicate thousand years. Numbers on the nodes are the point time-estimate corresponding to the median height of the node.

Thousand years before present

Supplementary Figure 6. BEAST result of the MTBC-185 model in which we assume a priori that the ancestor of MTBC existed sometime 185 kya. The numbers on the axis indicate thousand years. Numbers on the nodes are the point time-estimate corresponding to the median height of the node.

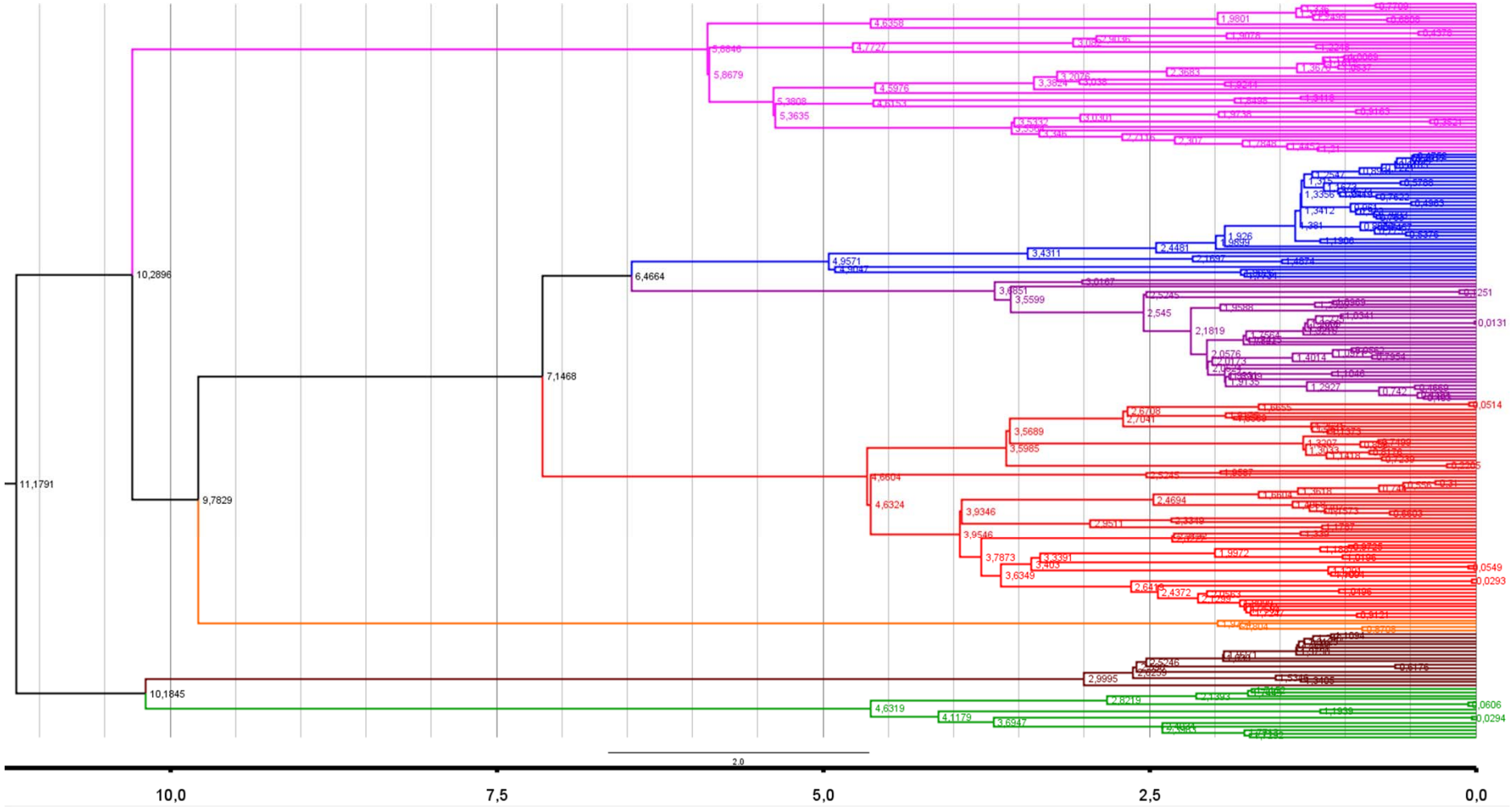

Supplementary Figure 7. BEAST result of the MTBC-10 model in which we assume a priori that the ancestor of MTBC existed sometime 10 kya. The numbers on the axis indicate thousand years. Numbers on the nodes are the point time-estimate corresponding to the median height of the node.

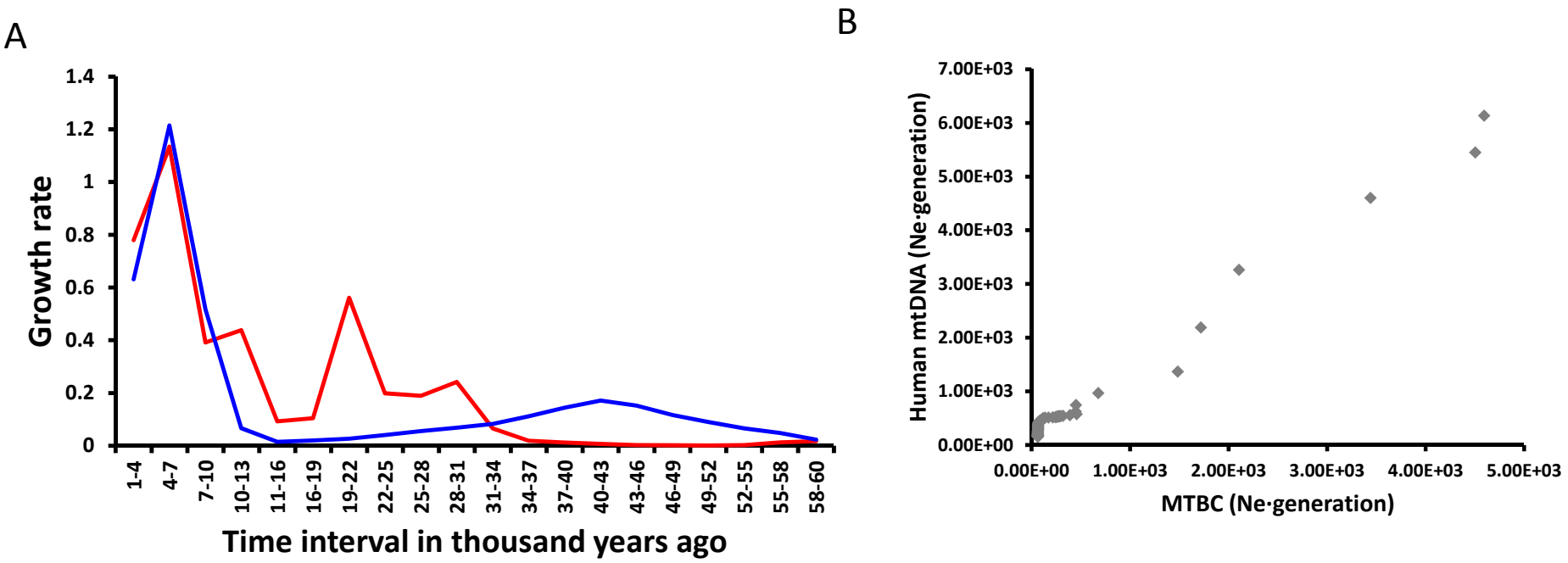

Supplementary Figure 8. (A) Growth rate calculated as described in Supplementary Methods for the MTBC-70 (red) and the corresponding human mtDNA dataset (blue). (**B**) Dot-plot correlation between the estimated population size of the MTBC and human mtDNA skyline curves using the median values.

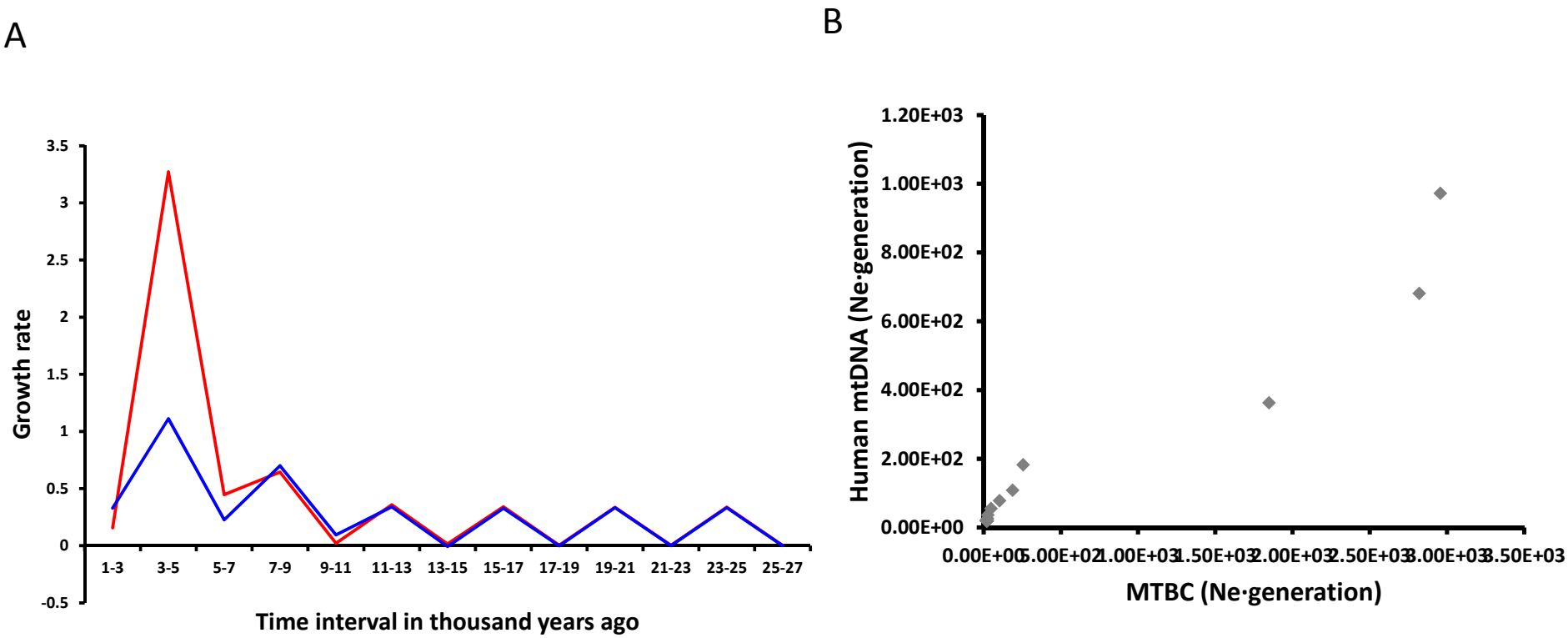

Supplementary Figure 9. (**A**) Growth rate calculated as described in Supplementary Methods for the MTBC Lineage 2 dataset (red) and the corresponding East Asian human mtDNA dataset (blue). (**B**) Dot-plot correlation between the estimated population size of the MTBC and human mtDNA skyline curves using the median values.

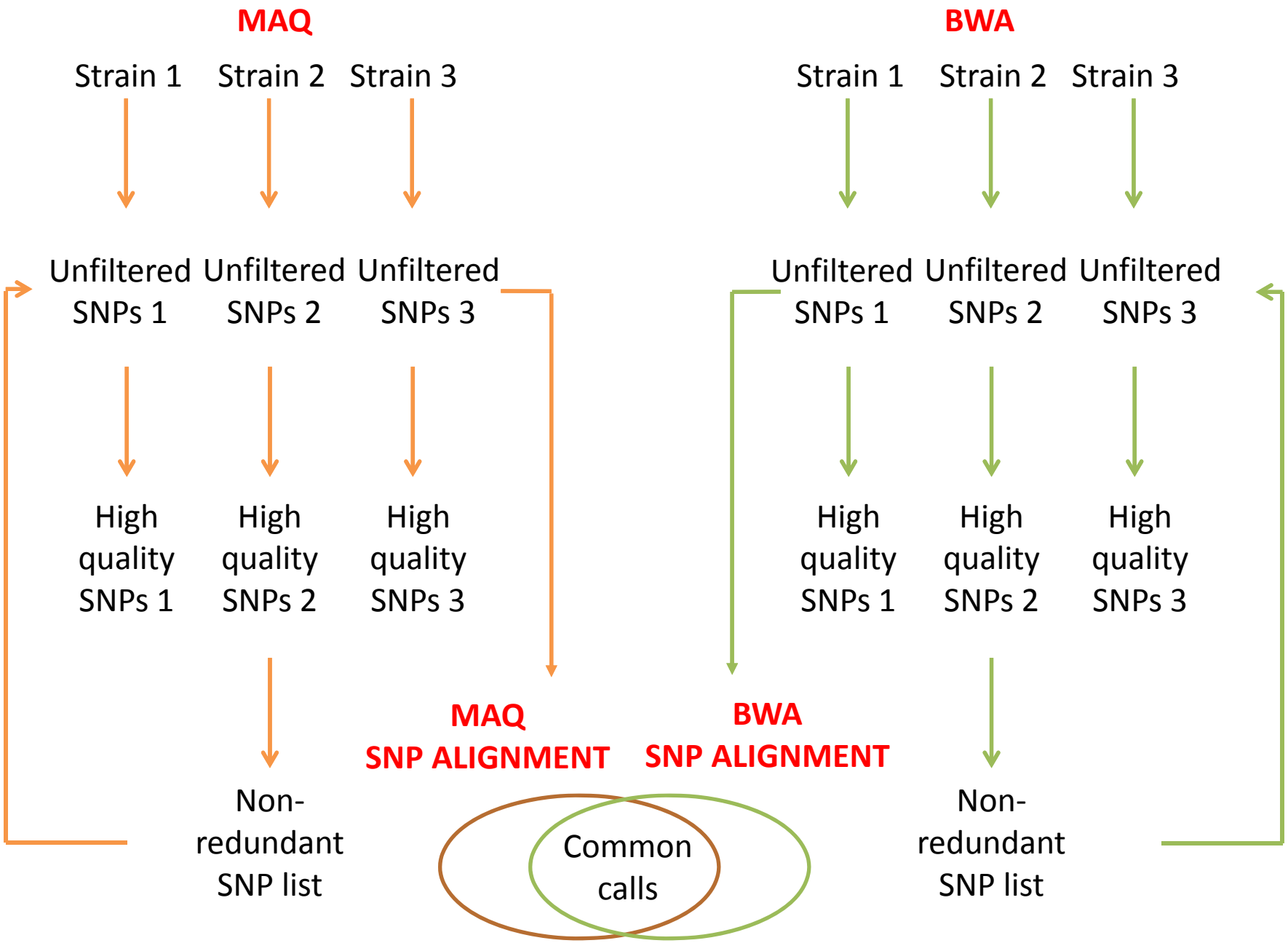

Supplementary Figure 10. Bioinformatic analysis pipeline used to call MTBC SNPs and extract alignments after MAQ and BWA analyses.

Supplementary Table 7. Number of MTBC positions with SNPs called both by MAQ and BWA sorted by various criteria. Number of alleles (when two or more alleles are present in the same position), number of positions in which at least one strains has no coverage indicating probable deletion (gap) and number of positions in which there is complete allele information for all strains (no gaps or heterozygous calls). Indicated in red are the variable nucleotide positions used for the downstream analyses.

MAQ vs. BWA common SNP calls	2 alleles	3-4 alleles
Core	30,303	189
Gaps	3,864	26
Heterozygous	272	1
Gaps and heterozygous	105	7

Supplementary Note

Ethical statement about the MTBC strains used in this study

The majority of MTBC strains used in this study came from previously established reference collections[1–3]. Strains from Nepal and China were collected through ongoing molecular epidemiological studies. Written informed consent was obtained from all patients. The studies were ethically approved by the Nepal Health Research Council and the Ethics Committee of the Canton of Basel (EKBB), Switzerland (Nepalese study), and by the Ethics Committee of the Shanghai Municipal Centre for Disease Control, Shanghai, China (Chinese study).

SNP calling after MAQ and BWA mapping

In the case of MAQ, we called the individual SNPs using default settings (minimum read depth 3, minimum consensus quality 20). In the case of BWA, we called SNPs by parsing the mapping output with SAMTOOLS[4] and keeping those SNPs that were more likely to be true SNPs (minimum mapping quality 20, maximum read depth 500). In each case, we generated a non-redundant list of variable positions called with high confidence in at least one strain and recovered the base call in all other strains as depicted in Supplementary Figure 10. Once we had the two lists of putative high confidence calls, we crossed the two lists and kept those calls that fulfilled the following criteria: 1) they were common to both lists, 2) there were no more than two alleles at that particular position, 3) they did not involve heterozygous calls, as these are more likely to represent mapping errors (only positions with deletions were kept), and 4) the position was not in a repetitive or mobile element. We used ANNOVAR[5] and custom annotation tools to describe each polymorphic position. For a workflow showing the calling approach used to get the final alignments see Supplementary Figure 10 and

Supplementary Table 7. The SNPs identified by both mapping approaches are listed in Supplementary Table 2.

Phylogenetic analyses

Both Maximum-likelihood and Neighbour-joining methods were used to infer the phylogenetic relationships between the taxa. Maximum-likelihood was implemented in RAXML[6] using GTR as a model of nucleotide substitution and 4 gamma rate categories correction. The Neighbour-joining method was based on Tamura-Nei distances as implemented in MEGA 5.0[7]. In both cases, clade support was determined using 1000 bootstrap pseudo-replicates. In both cases, the resulting phylogenies were largely congruent. In the case of the mitochondrial dataset, the limited phylogenetic information of the mitochondrial genomes and the presence of some known homoplasies[8] led to some incongruence between the two reconstruction methods. However, coalescent analyses are not expected to be affected by this as they integrate over all the possible phylogenies. Given the large number of taxa analyzed, we used FastTree[9] to derive the Maximum-likelihood phylogeny of the human mtDNA dataset. Unlike RAXML, FastTree does not implement a full Maximum-likelihood approach, but it has been shown to be more accurate and faster than other Maximum-likelihood approaches when applied to large datasets.

To identify homoplastic sites, we mapped the SNPs onto the MTBC phylogeny used to reconstruct the phylogeny and applied the ancestral reconstruction option using parsimony available in MESQUITE[10]. The positions that did not fit the phylogeny were recorded as homoplastic. To delineate different groupings among MTBC strains, we performed a principal component analysis using STATA s.e.m. version 10[11]. The three

first components were introduced in SigmaPlot 12.0[12] to generate a 3D scatter plot graph.

Phylogeographic analyses

The Bayesian stochastic search variable selection (BSSVS) implemented in BEAST was run after defining character states for each taxon, which in this case referred to geographic locations. The variable stochastic search procedure is also suitable for the case in which no outgroup is used as in our case[13]. *M. canettii* is most closely related to MTBC but it is a different species influenced by different evolutionary and ecological processes than MTBC[14,15]. Moreover, it is almost exclusively associated with East Africa, which would bias the result of the phylogeographic analyses. The configuration used for the BEAST runs are explained below.

RASP implements two different methods. A parsimony-based method (S-DIVA) minimizes the cost of adding new ranges in the ancestral nodes. In this analysis a maximum of two ancestral areas per node were allowed for range reconstruction. The second method is a full hierarchical Bayesian approach assuming no prior information about ancestral distributions; for this analysis ten different chains during 500 thousand generations were run.

BEAST skyline analyses

A Bayesian skyline model was used to look for changes in the effective population size per generation in each scenario estimated in 10 different intervals. A skyline plot measures the changes in population size using the number of coalescent events estimates at each interval. In all cases, we ran 6-12 chains of 50E6 generations sampled every 10E3 to assure independent convergence of the chains. Convergence was assessed using Tracer, ensuring all relevant parameters reached an effective sample size of >100.

The final skyline for the MTBC-70 scenario was generated by specifying two prior time points with the aim of reducing uncertainty around the dating and focusing only on the time of maximum expansion. We defined the height of the complex as 70 kya allowing +/- 5kya in a normal distribution, and we used 65 +/- 2 kya at the point of split of MTBC Lineage 1, after corroborating the concordance of both scenarios. To obtain the skyline plot for Lineage 2 strains, we used the dating of the most recent common ancestor of the Lineage 2 as derived from the MTBC-70 analysis (32 +/- 5 kya) as the prior input and ran BEAST using the same parameters as described above. To look at the correlation between the isolates sampling year and divergence we used Path-O-Gen.

To compare the MTBC and human mtDNA skyline plots and asses their correlation, we interpolated the values of the curve every one thousand years for MTBC-70 and mtDNA skyline curves from the median values and calculated the Spearman correlation coefficient using STATA s.e.m. version 10[11]. We also calculated for each skyline plot the growth rate every four thousand years for the global MTBC and mtDNA Neolithic datasets, and every three thousand years for the East Asia analyses. The growth rate formula used was as in Gignoux *et al.*[16]:

$$r_{(0-t)} = \frac{\ln(N_t / N_0)}{t_{0-t}}$$

where r refers to the growth rate between time 0 and time t, N_t refers to the median population size from the skyline plot at time t, N_0 refers to the median population size from the skyline plot at time 0, and t_{0-t} to the time span between both events.

Correlation between time since most recent common ancestor and predicted substitution rate in bacteria

For Figure 4 we searched the bibliography for bacterial genome datasets sequenced with a similar technology, analyzed with BEAST and that are predicted to have a most recent common ancestor at different age depth[21-27]. The mean time span since most recent common ancestor as reported in these different publications was used. Note that for some of them the age of the group of interest reported in the main text of the corresponding publication and the time span used in Figure 4 doesn't correlate, this is because the substitution rate reported many times include an outgroup not just the group of interest.

1. Hershberg, R. *et al.* High functional diversity in *Mycobacterium tuberculosis* driven by genetic drift and human demography. *PLoS Biology* **6**, e311 (2008).

2. Wirth, T. *et al.* Origin, spread and demography of the *Mycobacterium tuberculosis* Complex. *PLoS Pathogens* **4**, e1000160 (2008).

3. Gagneux, S. *et al.* Variable host–pathogen compatibility in *Mycobacterium tuberculosis*. *Proceedings Proc. Natl. Acad. Sci. U.S.A.* **103**, 2869–2873 (2006).

4. Li, H. *et al.* The Sequence Alignment/Map format and SAMtools. *Bioinformatics (Oxford, England)* **25**, 2078–9 (2009).

5. Wang, K., Li, M. & Hakonarson, H. ANNOVAR: functional annotation of genetic variants from high-throughput sequencing data. *Nucleic Acids Res.* **38**, e164–e164 (2010).

6. Stamatakis, A. RAxML-VI-HPC : maximum likelihood-based phylogenetic analyses with thousands of taxa and mixed models. *Bioinformatics* **22**, 2688–2690 (2006).

7. Tamura, K. *et al.* MEGA5 : Molecular evolutionary genetics analysis using maximum likelihood , evolutionary distance , and maximum parsimony methods research resource. *Mol. Biol. and Evol.* **28**, 2731–2739 (2011).

8. Gonder, M. K. *et al.* Whole-mtDNA genome sequence analysis of ancient African lineages. *Mol. Biol. and Evol.* **24**, 757–68 (2007).

9. Price, M. N., Dehal, P. S. & Arkin, A. P. FastTree 2 – Approximately maximum-likelihood trees for large alignments. *PLoS ONE* **5**, (2010).

10. Maddison, W. P. and D.R. Maddison. 2011. Mesquite: a modular system for evolutionary analysis. Version 2.75 http://mesquiteproject.org.

11. StataCorp. 2007. Stata Statistical Software: Release 10. College Station, TX: StataCorp LP.

12. SigmaPlot 12.0 (Systat Software, Inc., San Jose California USA, www.sigmaplot.com).

13. Lemey, P., Rambaut, A., Drummond, A. J. & Suchard, M. A. Bayesian phylogeography finds its roots. *PLoS Comp. Biol.* **5**, e1000520 (2009).

14. Gutierrez, M. C. *et al.* Ancient Origin and Gene Mosaicism of the Progenitor of *Mycobacterium tuberculosis*. *PLoS Pathogens* **1**, e5 (2005).

15. Jang, J. *et al.* Horizontally acquired genomic islands in the tubercle bacilli. *Trends Microbiol.* **16**, 303-308 (2008).

16. Gignoux, C. R., Henn, B. M. & Mountain, J. L. Rapid, global demographic expansions after the origins of agriculture. *Proceedings Proc. Natl. Acad. Sci. U.S.A.* **108**, 6044-6049 (2011).

17. Comas, I. *et al.* Human T cell epitopes of *Mycobacterium tuberculosis* are evolutionarily hyperconserved. *Nat. Genet.* **42**, 498-503 (2010).

18. Casali, N. *et al.* Microevolution of extensively drug-resistant tuberculosis in Russia. *Genome Re.* **4**, 735-745 (2012).

19. Comas, I. *et al.* Whole-genome sequencing of rifampicin-resistant *Mycobacterium tuberculosis* strains identifies compensatory mutations in RNA polymerase genes. *Nat. Genet.* **44**, 106-110 (2012).

20. Gardy, J. *et al.* Whole-genome sequencing and social-network analysis of a tuberculosis outbreak. *N. Engl. J. Med.* **364**, 730-739 (2011).

21. Kennemann, L. *et al. Helicobacter pylori* genome evolution during human infection. *Proceedings Proc. Natl. Acad. Sci. U.S.A.* **108**, 5033-5038 (2011).

22. He, M. *et al.* Emergence and global spread of epidemic healthcare-associated *Clostridium difficile*. *Nat. Genet.* **45**, 1–6 (2012).

23. Holt, K. E. *et al. Shigella sonnei* genome sequencing and phylogenetic analysis indicate recent global dissemination from Europe. *Nat. Genet.* **44**, 1056-1059 (2012).

24. Mutreja, A. *et al.* Evidence for several waves of global transmission in the seventh cholera pandemic. *Nature* **477**, 462–465 (2011).

25. Bos, K. I. *et al.* A draft genome of *Yersinia pestis* from victims of the Black Death. *Nature* **478**, 506-510 (2011).

26. Harris, S. R. *et al.* Evolution of MRSA During Hospital Transmission and Intercontinental Spread. *Science* **327**, 469–474 (2010).

27. Croucher, N. J. *et al.* Rapid Pneumococcal Evolution in Response to Clinical Interventions. *Science* **331**, 430–434 (2011).

28. Quintana-Murci L. *et al.* Where west meets east: the complex mtDNA landscape of the southwest and Central Asian corridor. *Am J Hum Genet.* **74**, 827-45 (2004).

29. Wang HW. *et al.* Mitochondrial DNA evidence supports northeast Indian origin of the aboriginal Andamanese in the Late Paleolithic. *J Genet Genomics.* **38**, 117-22 (2011).

30. Peng MS. *et al.* Tracing the Austronesian footprint in Mainland Southeast Asia: a perspective from mitochondrial DNA. *Mol Biol Evol.* **27**, 2417-30 (2010).

31. Xue F. *et al.* A spatial analysis of genetic structure of human populations in China reveals distinct difference between maternal and paternal lineages. *Eur J Hum Genet.* **16**, 705-17 (2008).

32. Salas A. *et al.* Mitochondrial echoes of first settlement and genetic continuity in El Salvador. *PLoS One.* **4**, e6882 (2009).

33. Msaidie S. *et al.* Genetic diversity on the Comoros Islands shows early seafaring as major determinant of human biocultural evolution in the Western Indian Ocean. *Eur J Hum Genet.* **19**, 89-94 (2011).

34. Kivisild T. *et al.* Ethiopian mitochondrial DNA heritage: tracking gene flow across and around the gate of tears. *Am J Hum Genet.* **5**, 752-70 (2004).

35. Tishkoff SA. *et al.* History of click-speaking populations of Africa inferred from mtDNA and Y chromosome genetic variation. *Mol Biol Evol.* **24**, 2180-95 (2007).

36. Ottoni C. *et al.* Mitochondrial analysis of a Byzantine population reveals the differential impact of multiple historical events in South Anatolia. *Eur J Hum Genet.* **19**, 571-6 (2011).

37. Fendt L. *et al.* MtDNA diversity of Ghana: a forensic and phylogeographic view. *Forensic Sci Int Genet.* **6**, 244-9(2012).

38. Hill C. *et al.* A mitochondrial stratigraphy for island southeast Asia. *Am J Hum Genet.* **80**, 29-43 (2007).

39. Asgharzadeh *et al.* Molecular diversity of mitochondrial DNA in Iranian Azeri ethnicities vis-a-vis other Azeris in Asia. Iran. *J. Biotechnol.* **2**, 120-125 (2011).

40. Tanaka M. *et al.* Mitochondrial genome variation in eastern Asia and the peopling of Japan. *Genome Res.* 2004 **14**, 1832-50 (2004).

41. Bodner M. *et al.* Southeast Asian diversity: first insights into the complex mtDNA structure of Laos. *BMC Evol Biol.* **11**,49 (2011).

42. Green LD, Derr JN, Knight A. mtDNA affinities of the peoples of North-Central Mexico. *Am J Hum Genet.* **66**, 989-98 (2000).

43. Merriwether DA. *et al.* mtDNA variation indicates Mongolia may have been the source for the founding population for the New World. *Am J Hum Genet.* **59**, 204-12 (1996).

44. Fornarino S. *et al.* Mitochondrial and Y-chromosome diversity of the Tharus (Nepal): a reservoir of genetic variation. *BMC Evol Biol.* **9**,154 (2009).

45. Nuñez C *et al.* Reconstructing the population history of Nicaragua by means of mtDNA, Y-chromosome STRs, and autosomal STR markers. *Am J Phys Anthropol.* **143**, 591-600 (2010).

46. Medeiros S. , *et al.* Haplogroup H Sub-Lineages with Mitochondrial SNPs. *Forensic Science International: Genetics Supplement Series* **1**, 285-286 (2008).

47. Martínez-Cruzado JC. *et al.* Reconstructing the population history of Puerto Rico by means of mtDNA phylogeographic analysis. *Am J Phys Anthropol.* **128**, 131-55 (2005).

48. Rosa A. *et al.* MtDNA profile of West Africa Guineans: towards a better understanding of the Senegambia region. Ann Hum Genet. 2004 Jul;68(Pt 4):340-52. Erratum in: Ann Hum Genet. 2005 Jul;69(Pt 4):499. *Ann Hum Genet.* **68**, 658 (2004).

49. Bosch E. *et al.* Paternal and maternal lineages in the Balkans show a homogeneous landscape over linguistic barriers, except for the isolated Aromuns. *Ann Hum Genet.* **70**, 459-87 (2006).

50. Jackson BA. *et al.* Mitochondrial DNA genetic diversity among four ethnic groups in Sierra Leone. *Am J Phys Anthropol.* **128**, 156-63 (2005).

51. Jin HJ, Tyler-Smith C, Kim W. The peopling of Korea revealed by analyses of mitochondrial DNA and Y-chromosomal markers. *PLoS One.* **4**, e4210 (2009).

52. Metspalu M. *et al.* Most of the extant mtDNA boundaries in south and southwest Asia were likely shaped during the initial settlement of Eurasia by anatomically modern humans. *BMC Genet.* **5**, 26 (2004).

53. Zimmermann B. *et al.* Forensic and phylogeographic characterization of mtDNA lineages from northern Thailand (Chiang Mai). Int *J Legal Med.* **123**, 495-501 (2009).

54. Tabbada KA. *et al.* Philippine mitochondrial DNA diversity: a populated viaduct between Taiwan and Indonesia? *Mol Biol Evol.* **27**, 21-31 (2010).

55. Torroni A. *et al.* Classification of European mtDNAs from an analysis of three European populations. *Genetics.* **144**, 1835-50 (1996).

56. Jin HJ, Tyler-Smith C, Kim W. The peopling of Korea revealed by analyses of mitochondrial DNA and Y-chromosomal markers. *PLoS One.* **4**, e4210 (2009).